Materials Science and Engineering Publications   Materials Science and Engineering

Synthesis and Characterization of Hydrated Rubidium Thio-hydroxosilicogermanates Using Mechanochemical Hydrothermal Synthesis

Carly R. Nelson
Iowa State University

Sarah Olson
Iowa State University

Steven A. Poling
Iowa State University

Steve W. Martin
Iowa State University, swmartin@iastate.edu

Synthesis and Characterization of Hydrated Rubidium Thio-hydroxosilicogermanates Using Mechanochemical Hydrothermal Synthesis

Abstract

The synthesis, structure, and proton conductivity of the hydrated thio-hydroxosilicogermanates $RbzGexSi1-xSz(OH)4-z \cdot yH_2O$ ($2 \leq z \leq 3$; $0 < y < 1.7$) are reported. X-ray diffraction indicates that the $z = 2$ materials are amorphous and show no unreacted starting materials, which is consistent with the mechanochemical hydrothermal evaporation−precipitation synthesis method. Infrared spectroscopy shows a fully reacted system where both silicon and germanium central anions have vibrational modes at 950, 780, 667, and 450 cm-1 associated with asymmetric modes for Si−O, Ge−O, Si−S, and Ge−S chemical bonds, respectively. O−H stretching and bending modes are present at 3370 and 1655 cm-1, respectively, with the intensities of both modes decreasing with the addition of SiO_2. Raman spectroscopy reveals symmetric stretching modes of the Ge−S unit at 420 cm-1. A new peak appears at 460 cm-1 with the substitution of Si^{4+} for Ge^{4+}. There are weak peaks above 460 cm-1 that can be attributed to H_2O and O−H libration modes. Thermogravimetric analysis shows that water loss begins above the synthesis temperature of 75 °C. All water is lost by 300 °C which is consistent with the onset of the loss of conductivity. Alternating current impedance spectroscopy measurements performed on low-pressure sealed pellets show conductivity values ranging from 10-5 to 10-2.5 S/cm from 100 to 260 °C, respectively. Maximum conductivity values of 10-4.5 and 10-3.5 S/cm at 120 °C are obtained for $2RbSH + 0.9GeO_2 + 0.1SiO_2 + 0.8H_2O$ and $3RbSH + 0.9GeO_2 + 0.1SiO_2 + 1.1H_2O$, respectively. a.c. impedance experiments under humidified conditions resulted in large increases in the proton conductivity at low temperatures. For $x = 0.9$ and 0.8 for the $2RbSH + xGeO_2 + (1−x)SiO_2 +yH_2O$ samples, the humidified d.c. conductivity was 10-4 S/cm at 60 °C, up from 10-8 S/cm for samples measured under dry nitrogen. The effects of water and SiO_2 content on the proton conductivity are also discussed.

Disciplines

Ceramic Materials | Inorganic Chemistry | Materials Chemistry | Materials Science and Engineering

Synthesis and Characterization of Hydrated Rubidium Thio-hydroxosilicogermanates Using Mechanochemical Hydrothermal Synthesis

Carly R. Nelson, Sarah Olson, Steven A. Poling, and Steve W. Martin*

Department of Materials Science and Engineering, 2220 Hoover Hall, Iowa State University of Science and Technology, Ames, Iowa 50011

The synthesis, structure, and proton conductivity of the hydrated thio-hydroxosilicogermanates $Rb_zGe_xSi_{1-x}S_z(OH)_{4-z} \cdot yH_2O$ ($2 \leq z \leq 3$; $0 < y < 1.7$) are reported. X-ray diffraction indicates that the $z = 2$ materials are amorphous and show no unreacted starting materials, which is consistent with the mechanochemical hydrothermal evaporation−precipitation synthesis method. Infrared spectroscopy shows a fully reacted system where both silicon and germanium central anions have vibrational modes at $\sim$950, $\sim$780, $\sim$667, and $\sim$450 cm^{-1} associated with asymmetric modes for Si−O, Ge−O, Si−S, and Ge−S chemical bonds, respectively. O−H stretching and bending modes are present at $\sim$3370 and 1655 cm^{-1}, respectively, with the intensities of both modes decreasing with the addition of SiO_2. Raman spectroscopy reveals symmetric stretching modes of the Ge−S unit at $\sim$420 cm^{-1}. A new peak appears at $\sim$460 cm^{-1} with the substitution of Si^{4+} for Ge^{4+}. There are weak peaks above $\sim$460 cm^{-1} that can be attributed to H_2O and O−H libration modes. Thermogravimetric analysis shows that water loss begins above the synthesis temperature of $\sim$75 °C. All water is lost by $\sim$300 °C which is consistent with the onset of the loss of conductivity. Alternating current impedance spectroscopy measurements performed on low-pressure sealed pellets show conductivity values ranging from 10^{-5} to $10^{-2.5}$ S/cm from $\sim$100 to 260 °C, respectively. Maximum conductivity values of $10^{-4.5}$ and $10^{-3.5}$ S/cm at 120 °C are obtained for 2RbSH + $0.9GeO_2$ + $0.1SiO_2$ + $0.8H_2O$ and 3RbSH + $0.9GeO_2$ + $0.1SiO_2$ + $1.1H_2O$, respectively. a.c. impedance experiments under humidified conditions resulted in large increases in the proton conductivity at low temperatures. For $x = 0.9$ and 0.8 for the 2RbSH + $xGeO_2$ + $(1-x)SiO_2$ + yH_2O samples, the humidified d.c. conductivity was $\sim$$10^{-4}$ S/cm at 60 °C, up from $\sim$$10^{-8}$ S/cm for samples measured under dry nitrogen. The effects of water and SiO_2 content on the proton conductivity are also discussed.

Introduction

The need for alternative energy sources has increased greatly over the past few years due to high gasoline prices and stricter pollution regulations. Research into H_2−O_2 fuel cells operating in the intermediate temperature range ($\sim$100−300 °C) provides possible solutions to these problems with H_2−O_2 fuel cells having zero emission and using hydrogen and oxygen as fuels. The heart of the H_2−O_2 fuel cell is the proton-exchange membrane (PEM) which works to transport proton species from the anode to the cathode, thus creating electricity. A common material for the PEM is Nafion, a hydrated perfluorinated polymer, which has a proton conductivity of $\sim$$10^{-0.77}$ S/cm at 80 °C under heavily hydrated conditions. There are various other polymers which have proton conductivities high enough for fuel cell applications.[1−4] Our work has been performed to develop a material for the PEM that does not rely on such high levels of hydration to have high proton conductivity.

Our previous work on ceramic materials, which are more thermally stable than polymeric materials, has resulted in proton conductivities of $\sim$$10^{-2}$ S/cm at 120 °C and thermal stabilities up to $\sim$300 °C for hydrated heavy alkali thio-hydroxogermanates.[5,6] These high proton-conducting materials are of the form $M_xGeS_x(OH)_{4-x} \cdot yH_2O$ where M = Na, K, Rb, Cs, $1 \leq x \leq 4$ and $0 < y < 8$. It has been shown that mixed oxysulfide systems have higher ionic conductivities than either their oxide or sulfide counterparts and suggests their promise as PEMs for use in the intermediate temperature range.[7−9] These alkali thio-hydroxogermanates have also been found to be reversibly dehydrated and hydrated according to vibrational spectroscopy investigations.[10] Other work has also been performed on an all oxide systems $M_3HGe_7O_{16} \cdot xH_2O$ where M = Li, Na, K, Rb, Cs and $x = 0$−6.[11,12] The maximum proton conductivity reached for these

(1) Hoogers, G. *Fuel Cell Technology Handbook*; CRC Press: London, 2003.
(2) Kreuer, K. D. *Chem. Mater.* **1996**, *8*, 610.
(3) Herz, H. G.; Krueur, K. D. *Electrochim. Acta* **2003**, *48*, 2165.
(4) Kreuer, K. D. *J. Membr. Sci.* **2001**, *185*, 29.
(5) Poling, S. A.; Nelson, C. R.; Martin, S. W. *Chem. Mater.* **2005**, *17*, 1728.
(6) Poling, S. A.; Nelson, C. R.; Martin, S. W. *Mater. Lett.* **2006**, *60,* 23.
(7) Tatsumisago, M.; Hirai, K. *Solid State Ionics* **1996**, *86−88*, 487.
(8) Hayashi, A.; Hirai, K.; Tatsumisago, M.; Takahashi, M.; Minami, T. *Solid State Ionics* **1996**, *86−88*, 539.
(9) Minami, T.; Hayashi, A.; Tatsumiasago, M. *Solid State Ionics* **2000**, *36−137*, 1015.
(10) Karlsson, M.; Nelson, C. R.; Martindale, C. A.; Martin, S. W.; Matic, A.; Börjesson, L. *Solid State Ionics* **2006**, *177*, 1009.
(11) Feng, S.; Tsai, M.; Greenblatt, M. *Chem. Mater.* **1992**, *4,* 388.

Hydrated Rubidium Thio-hydroxosilicogermanates

Chem. Mater., Vol. 18, No. 26, 2006 6437

materials was $\sim 10^{-3}$ S/cm at ~ 300 °C for $Rb_3HGe_7O_{16}\cdot 4H_2O.$[12]
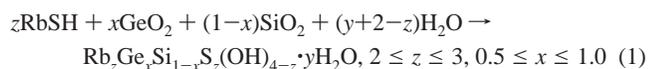
To further increase the ionic conductivity, Si^{4+} was substituted for Ge^{4+} which was expected to weaken the electrostatic interaction between mobile cations, resulting in an increase in the cation conductivity. Materials of the form $M_3HGe_{7-m}Si_mO_{16}\cdot xH_2O$ where M = K, Rb, Cs, $0 < m < 3$ and $x = 0-4$ were synthesized and were observed to show an increase in the cation conductivity and a decrease in the activation energy with increasing silicon content.[13]

A mechanochemical hydrothermal reaction method has been used to promote reaction of the silicon dioxide in water. This method has previously been shown to work in the $MgO-SiO_2$ and $Mg(OH)_2-SiO_2$ system where amorphous products were obtained through hydrothermal reactions.[14,15] For example, Avvakumov et al. was able to show that hydrated oxides react faster mechanochemically than for anyhydrous oxide mixtures.[16,17]

In this work, we expand on the previously synthesized alkali thio-hydroxogermanates of the form M_xGeS_x-$(OH)_{4-x}\cdot yH_2O.$ We have specifically focused on the rubidium system which was shown to have the best combination of proton conductivity and thermal stability. In an effort to improve the thermal stability and proton conductivity by substituting Si^{4+} for Ge^{4+}, hydrothermal mechanochemical synthesis technique will be investigated to increase the reactivity of SiO_2 in water.

Experimental Section

Sample Preparation. Samples of the form $Rb_xGe_zSi_{(1-z)}S_x(OH)_{4-x}\cdot yH_2O$ were prepared by placing 0.5 g batches of stoichiometric amounts of $RbSH$,[18] commercial quartz-type GeO_2 (Cerac 99.999%, ~ 325 mesh), and amorphous SiO_2 (Alfa 99.9%) in 5 mL of deionized (DI) water in a Fritsch Pulverisette-6 planetary mono mill with 10 ZrO_2 milling balls, 10 mm in size, in a ZrO_2 bowl. Planetary milling was used to decrease the particle size, thus increasing the surface area available to increase the reaction rate. The corresponding reactions may be written as:

$$zRbSH + xGeO_2 + (1-x)SiO_2 + (y+2-z)H_2O \rightarrow$$
$$Rb_zGe_xSi_{1-x}S_z(OH)_{4-z}\cdot yH_2O, \; 2 \leq z \leq 3, \; 0.5 \leq x \leq 1.0 \quad (1)$$

Samples were milled for 2 h at 200 rpm and then transferred to a polypropylene jar on a hot plate at ~ 75 °C to dry. A dried film was deposited after allowing the excess water to evaporate at ~ 75 °C. Samples were then stored under a dry N_2 atmosphere where preparations for sample characterizations were performed.

Structural Characterizations. Structural investigations were performed using X-ray diffraction (XRD), infrared (IR) absorption, Raman scattering, and scanning electron microscope energy dispersive spectrometry (SEM-EDS). The powder XRD spectra were collected at 298 K with a Scintag XDS-2000 diffractometer using Cu Kα radiation ($\lambda = 1.54178$ Å), 40 kV, and 30 mA. Scans were performed between 20° and 60° 2θ using a 0.02° step size and a 0.5 s dwell time. Powdered samples were packed into a recessed square polycarbonate sample holder and covered with 0.001 in. thick Kapton (Polyimide) tape to seal out atmospheric moisture. The IR absorption spectra were collected at 298 K with a Bruker IFS 66 v/S spectrometer using 32 scans and 4 cm^{-1} resolution in both the mid-IR and far-IR regions. Translucent CsI pellets were prepared for transmission by mixing ~ 1 wt % of powder sample with CsI and pressing. The Raman scattering spectra were collected at 298 K with a Bruker FT-Raman RFS 100/S spectrometer using a 1064 nm Nd:YAG laser, 32 scans, 2 cm^{-1} resolution, and 300 mW of power focused on a ~ 0.1 mm diameter spot size. SEM-EDS measurements were performed using a Jeol JSM-6060LV system with an Inca EDS-7582. The samples were pressed into pellets and sputtered in gold (~ 5 nm) in a N_2 atmosphere.

Thermal Characterizations. Thermal mass loss measurements were performed with a Perkin-Elmer Thermogravimetric Analyzer TGA 7 (TGA). About 10 mg of sample was placed in an open aluminum sample pan. The sample was then heated at a rate of 10 °C/min from 50 to 500 °C using 20 mL/min flow of N_2 as the sample purge gas.

Conductivity Measurements. a.c. impedance data were collected with a Gamry PC4/750 potentiostat in the frequency range of 0.2 Hz to 100 kHz using 0.5 V amplitude on compacted powder samples. Hardened steel blocking electrodes with a 6.35 mm o.d. were pressed inside an undersized Teflon sleeve containing ~ 60 mg of sample. A pressure of ~ 562 MPa was applied to produce an average pellet thickness of ~ 0.4 mm. Constant pressure was maintained on the pellet during the measurement by the electrodes and an aluminum 'O'-frame insulated from the electrodes with Teflon. The pellet/electrode/frame assembly was contained inside a mullite cell that maintained about 1 atm of N_2. Hydrated impedance runs were performed by bubbling dry air ($\sim 0\%$ R.H. at STP) through a controlled temperature water bath ($T \sim 50$ °C). The bottom of the cell was placed into a custom-built crucible furnace and data were collected using increments of 10 °C after allowing the sample temperature to stabilize for 20 min. The d.c. conductivity values were determined from the intersection of the observed depressed semicircle and the low-frequency polarization "tale" in the Nyquist plot of the complex impedance.

Results and Discussion

Sample Preparation. Amorphous products were obtained which are consistent with the evaporation−precipitation synthesis method used. The resulting dried material was in the form of a translucent film. At room temperature in humidified air, the rubidium thio-hydroxosilicogermanates readily absorb water and are very soluble in water, similar to alkali salts. This strong affinity for water affects the stoichiometry of the final product in that different amounts of intercalated water can be present in the sample with slightly different experimental conditions. Under nonhumidified (dry) conditions, the samples are very stable and easily pressed into powder pellets.

Structural Characterizations: XRD. The powder XRD diffractograms indicate that the substitution of small amounts of Si^{4+} for Ge^{4+} results in a noncrystalline material for the $2RbSH + xGeO_2 + (1-x)SiO_2 + yH_2O$ samples which was observed for the previously synthesized alkali thio-hydroxogermanates.[5] Figure 1 shows the diffractograms for 2RbSH

(12) Feng, S.; Greenblatt, M. *Chem. Mater.* **1992**, *4*, 462.
(13) Feng, S.; Tsai, M.; Greenblatt, M. *Chem. Mater.* **1992**, *4*, 468.
(14) Temuujin, J.; Okada, K.; MacKenzie, K. J. D. *J. Solid State Chem.* **138**, 169.
(15) Liao, J.; Senna, M. *Thermochim. Acta* **1992**, *210*, 89.
(16) Avvakumov, E. G.; Kosova, N. V.; Devyatkina, E. T. *Neorg. Mater.* **1992**, *28*, 2176.
(17) Avvakumov, E. G.; Devyatkina, E. T.; Kosova, N. V. *J. Solid State Chem.* **1994**, *113*, 379.
(18) Martin, S.W.; Poling, S. A.; Sutherland, J. T. U.S. Patent application 10 627 584, 2003.
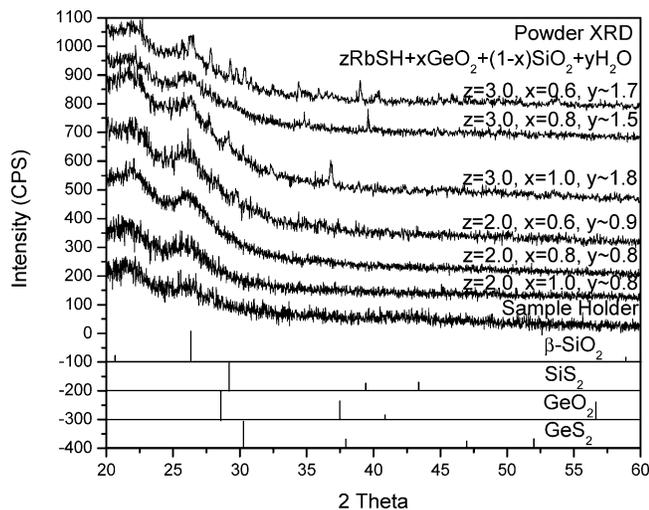
Figure 1. Powder XRD diffractograms for the as-prepared $2RbSH + xGeO_2 + (1-x)SiO_2 + nH_2O$ and $3RbSH + xGeO_2 + (1-x)SiO_2 + nH_2O$ ($x = 1.0, 0.8, 0.6$) samples. Scans were obtained from finely powdered samples covered with 0.001 in. thick Kapton (Polyimide) tape. An empty polycarbonate sample holder covered with tape is shown as a reference. Major peaks from crystalline β-SiO_2, SiS_2, GeO_2, and GeS_2 are also shown for reference.

$+ xGeO_2 + (1-x)SiO_2 + nH_2O$ ($x = 1.0, 0.8, 0.6$) and $3RbSH + xGeO_2 + (1-x)SiO_2 + nH_2O$ ($x = 1.0, 0.8, 0.6$). The samples were covered with a Polyimide tape to prevent sample hydration at room temperature. There were no observed peaks that were distinguishable from the polycarbonate holder background from 20° to 60° 2θ for the $2RbSH + xGeO_2 + (1-x)SiO_2 + nH_2O$ samples. There was no evidence of unreacted RbSH, GeO_2, SiO_2, or ZrO_2 from the milling bowl and ball media. Weak peaks were present for the $x = 0.8$ and $x = 0.6$ composition of the $3RbSH + xGeO_2 + (1-x)SiO_2 + nH_2O$ phase, perhaps indicating a semicrystalline structure. Crystalline β-SiO_2,[19] SiS_2,[20] GeO_2,[21] and GeS_2[22] are shown for reference. It does appear that there is a small percentage of crystalline products in the $3RbSH + xGeO_2 + (1-x)SiO_2 + nH_2O$ samples. The resulting XRD amorphous materials are consistent with the employed synthesis route of planetary milling and then evaporating− precipitating at ~75 °C. Crystalline products have been obtained for similar binary samples, $Na_2GeS_2(OH)_2\cdot5H_2O$ and $Na_3GeS_3(OH)\cdot8H_2O$, by using large amounts of acetone at room temperature to isolate the crystalline phases.[23,24] The proposed structural model is a metal anion, either germanium or silicon, tetrahedrally coordinated by sulfur anions and hydroxide ions. The sulfur anions are terminated by rubidium cations.

Structural Characterizations: IR. The IR spectra indicate a mixed system with both germanium and silicon bonding to both oxygen and sulfur and the presence of hydrated water. Figures 2 and 3 show the spectra for samples of the form $Rb_2(Ge_xSi_{1-x})S_2(OH)_2\cdot yH_2O$ and $Rb_3(Ge_xSi_{1-x})S_3$-

(19) Liu, X.; Su, W.; Zhao, X.; Wang, Y. *Mater. Lett.* **1993**, *18*, 234.
(20) Guseva, T.; Burdina, K.; Semenenko, K. *Moscow Univ. Chem. Bull.* **1991**, *46*, 90.
(21) Bolzan, A. A.; Fong, C.; Kennedy, B. J.; Howard, C. J. *Acta Crystallogr., Sect. B* **1997**, *53*, 373.
(22) Prewitt, C. T.; Young, H. S. *Science* **1965**, *149*, 535.
(23) Krebs, B.; Wallstab, H. *Z. Naturforsch.* **1981**, *36b*, 1400.
(24) Krebs, B.; Wallstab, H. *Inorg. Chim. Acta* **1981**, *54*, L123.

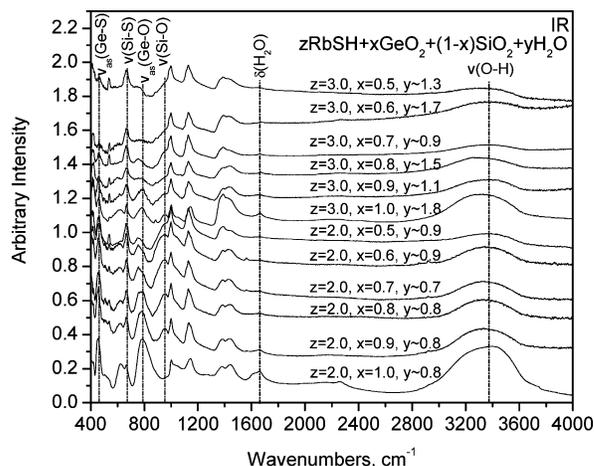**Figure 2.** Infrared absorption spectra for the as-prepared $zRbSH + xGeO_2 + (1-x)SiO_2 + nH_2O$ ($z = 2$ and 3, $0.5 \leq x \leq 1.0$). Vibrational modes located at ~950, 780, 667, and 450 cm^{-1} are attributed to Si−O$^-$, Ge−O$^-$, Si−S$^-$, and Ge−S$^-$ bond stretch vibrations. O−H stretching and bending vibrations are observed at ~3370 and 1655 cm^{-1}, respectively. H_2O and O−H liberation modes are present as sharp bands between 1446 and 534 cm^{-1}.[5]
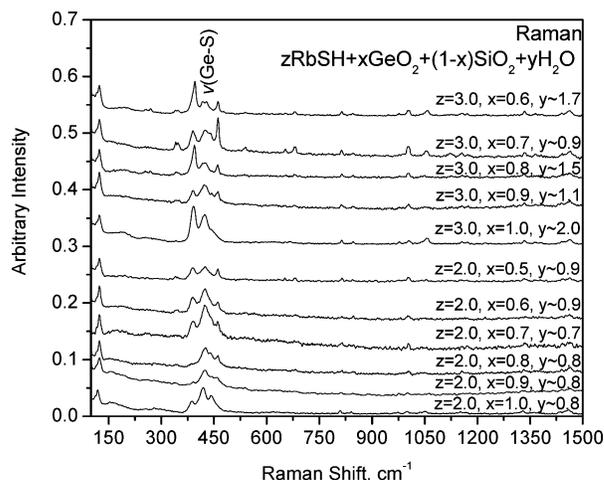

Figure 3. Raman scattering spectra for the as-prepared $zRbSH + xGeO_2 + (1-x)SiO_2 + nH_2O$ ($z = 2$ and 3, $0.5 \leq x \leq 1.0$). Stretching vibrations associated with the Ge−S$^-$ bond are located between 385 and 443 cm^{-1}. A vibrational mode at ~460 cm^{-1} is attributed to the substitution of Ge^{4+} by Si^{4+}. Sharp vibrational peaks above ~460 cm^{-1} may be attributed to H_2O and O−H rotary modes.

(OH)·yH_2O, respectively. The previously synthesized amorphous $2RbSH + GeO_2 + yH_2O$ is observed to have vibrations at ~450, 622, and 780 cm^{-1} associated with vibrations from asymmetric Ge−S$^-$, Ge−OH, and Ge−O$^-$, respectively.[5] Water bands associated with O−H stretching and H−O−H bending are observed at ~3370 and 1655 cm^{-1}, respectively. The doping of Si^{4+} for Ge^{4+} results in the addition of numerous vibrational modes. At $x = 0.9$, a band appears at ~950 cm^{-1}, which can be assigned to the asymmetric Si−O stretching of the Si−OH group.[14] This mode is observed to broaden as more silicon is added.[25] It is observed that as the concentration of GeO_2 decreases from $x = 0.9$ to $x = 0.6$, the intensity of the asymmetric stretching band at ~780 cm^{-1} decreases and shifts to lower wavenumbers, indicating stronger bonding. The intense asymmetric vibration associ-

(25) Kawakami, Y.; Ikuta, H.; Uchida, T.; Wakihara, M. *Thermochim. Acta* **1997**, *299*, 7.

Table 1. SEM-EDS Results Using a Jeol JSM-6060LV System with an Inca EDS-7582[a]

sample	Rb	Ge	Si	S	O
$2RbSH + 0.6GeO_2 + 0.4SiO_2$					
theoretical weight %	52.8	13.5	3.47	19.8	9.88
EDS weight %	50.3	22.7	4.79	15	7.16
$2RbSH + 0.8GeO_2 + 0.2SiO_2$					
theoretical weight %	51.4	17.5	1.69	19.3	9.61
EDS weight %	48.7	26.6	3.46	15.6	5.77
$3RbSH + 0.6GeO_2 + 0.4SiO_2$					
theoretical weight %	60.4	10.3	2.65	22.7	3.77
EDS weight %	54.9	12.7	3.68	17.2	11.5
$3RbSH + 0.8GeO_2 + 0.2SiO_2$					
theoretical weight %	59.2	13.4	1.3	22.2	3.69
EDS weight %	54.3	16.8	2.72	17.8	8.37

[a] Samples were pressed into 0.5 in. diameter pellets and sputtered in gold in a N_2 atmosphere.

ated with Ge−S$^-$ is observed to decrease in intensity with the reduction of germanium in the sample. The mode at ~667 cm^{-1} has previously been reported as the stretching vibration for the Si−S$^-$ bond.[25] The addition of SiO_2 also results in a decrease in the O−H stretching vibrations at ~3360 cm^{-1}, perhaps indicating that the retention of water in the sample is due to the presence of germanium, not silicon. In agreement with this, there is a very weak O−H bending mode at ~1655 cm^{-1} for the $x = 0.9$ of $2RbSH + xGeO_2 + (1-x)SiO_2 + yH_2O$, but it is observed to disappear with further additions of SiO_2. The O−H bending mode is present at ~1655 cm^{-1} for $x = 1.0$ to $x = 0.7$ for the $3RbSH + xGeO_2 + (1-x)SiO_2 + yH_2O$ samples, which indicates that higher concentrations of alkali lead to larger amounts of intercalated water.

Structural Characterizations: Raman. Figure 3 shows the corresponding Raman spectra for the as-prepared $zRbSH + xGeO_2 + (1-x)SiO_2 + yH_2O$ ($z = 2$ and 3, $0.5 \le x \le 1.0$) samples. The Raman spectra for $2RbSH + GeO_2 + yH_2O$ and $3RbSH + GeO_2 + yH_2O$ have been previously reported and show peaks between 483 and 358 cm^{-1} which are associated with stretching modes of terminal Ge−S$^-$ and bridging Ge−O−Ge units and of nonbridging Ge−O$^-$ (H$^+$) and Ge−O$^-$ (M$^+$) units.[5] The substitution of Si^{4+} for Ge^{4+} results in a new peak at ~460 cm^{-1}. It has previously been reported that the substitution of Si for Ge in GeS$_2$ units results in additional Raman lines between 450 and 550 cm^{-1}, perhaps explaining the evolution of the peak at ~460 cm^{-1}.[26] The intensity of the symmetric stretching Ge−S$^-$ mode at ~420 cm^{-1} is observed to decrease in intensity as the concentration of Si^{4+} increases. There does not appear to be a vibrational mode associated with bridging Ge−S−Ge modes (~340 cm^{-1}), which supports our proposed structure.[27]

Compositional Characterizations: SEM-EDS. Table 1 shows the results for the four samples investigated using X-ray diffraction, $2RbSH + 0.6GeO_2 + 0.4SiO_2$, $2RbSH + 0.8GeO_2 + 0.2SiO_2$, $3RbSH + 0.6GeO_2 + 0.4SiO_2$, and $3RbSH + 0.8GeO_2 + 0.2SiO_2$. The EDS results agree well with trends that are to be expected for the samples investigated. Within each system, the $xRbSH + 0.8GeO_2 + 0.2SiO_2$
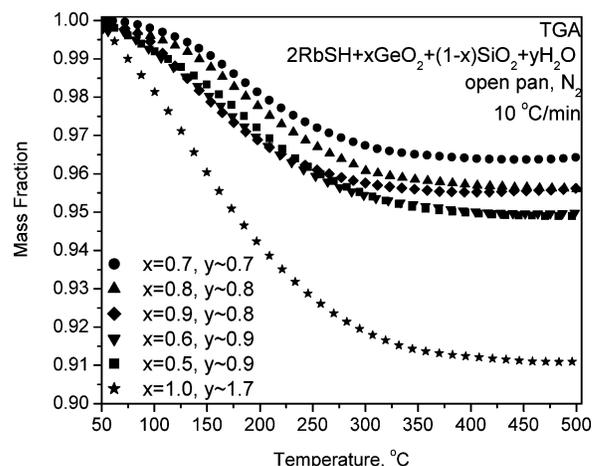
(26) Tenhover, M.; Hazle, M. A.; Grasselli, R. K. *Phys. Rev. B* **1983**, *28* (10), 5897.
(27) Kim, Y.; Saienga, J.; Martin, S. W. *J. Non-Cryst. Solids* **2005**, *351*, 3716.

Figure 4. TGA thermograms for the as-prepared $2RbSH + xGeO_2 + (1-x)SiO_2 + nH_2O$. Samples were placed in an open aluminum pan, heated at 10 °C/min, and purged with N_2. Continuous mass loss is observed above the synthesis temperature of ~75 °C with a change in the slope observed between 280 and 290 °C attributed to the formation of bridging oxygens.
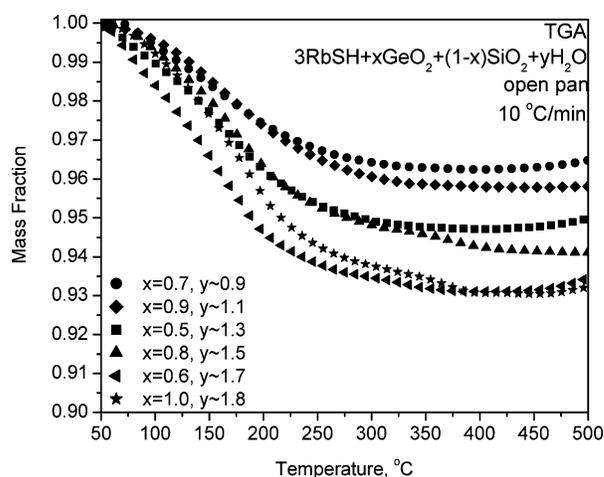

Figure 5. TGA thermograms for the as-prepared $3RbSH + xGeO_2 + (1-x)SiO_2 + nH_2O$. Samples were placed in an open aluminum pan, heated at 10 °C/min, and purged with N_2. Continuous mass loss is observed above the synthesis temperature of ~75 °C with a change in the slope observed between 240 and 270 °C attributed to the formation of bridging oxygens.

sample was found to have more germanium and less silicon than the corresponding $xRbSH + 0.6GeO_2 + 0.4SiO_2$. Larger errors were observed for the silicon and oxygen contents which were to be expected. Silicon is very light and present in such small amounts that accuracy is difficult. Errors were observed for oxygen because the exact amount of intercalated water upon exposing the samples to air momentarily and then placing under high vacuum is not known so theoretical calculations were performed assuming a completely dehydrated sample which would be consistent with the full removal of water under high vacuum.

Thermal Characterizations: TGA. Figures 4 and 5 present the TGA thermograms for the as-prepared $2RbSH + xGeO_2 + (1-x)SiO_2 + yH_2O$ and $3RbSH + xGeO_2 + (1-x)SiO_2 + yH_2O$, respectively. The calculations for the amount of water (·yH_2O) present in each sample were performed by assuming that all intercalated water was lost by the second inflection point. Continuous mass loss is observed above the preparation temperature of ~75 °C with open sample pans purged under a nitrogen atmosphere. Both
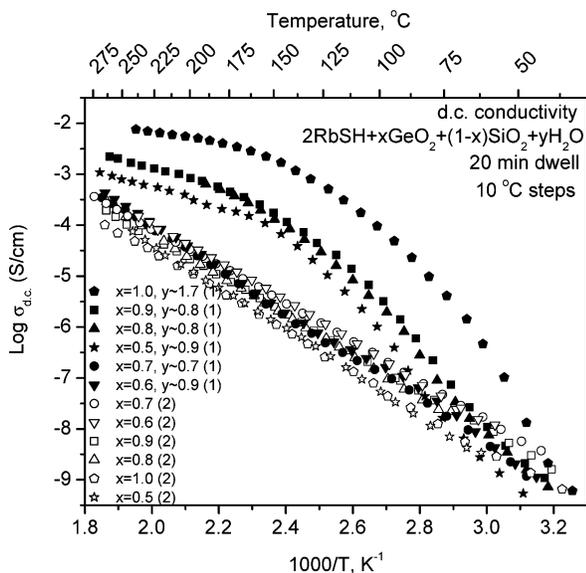
Figure 6. Arrhenius temperature-dependent plot of d.c. conductivity for the as-prepared $2RbSH + xGeO_2 + (1-x)SiO_2 + nH_2O$, both first and second heating cycles. Measurements were performed using 10 °C steps and 20 min stabilization times on compacted powder pellets sealed in a Teflon sleeve by hardened steel electrodes.

Figure 7. Arrhenius temperature-dependent plot of d.c. conductivity for the as-prepared $3RbSH + xGeO_2 + (1-x)SiO_2 + nH_2O$, both first and second heating cycles. Measurements were performed using 10 °C steps and 20 min stabilization times on compacted powder pellets sealed in a Teflon sleeve by hardened steel electrodes.

of the $x = 1$ samples for $2RbSH + xGeO_2 + (1-x)SiO_2 + yH_2O$ and $3RbSH + xGeO_2 + (1-x)SiO_2 + yH_2O$ have the highest amount of intercalated water. It was previously shown for the alkali thio-hydroxogermanates that the inflection point between 200 and 300 °C is attributed to the removal of molecular water associated with the hydrated cation shell.[5] A second inflection point around 400−450 °C is attributed to the thermal decomposition of hydroxyl groups and the formation of bridging oxygens.[5] A second inflection point is not easily observed for the $2RbSH + xGeO_2 + (1-x)$-$SiO_2 + yH_2O$ materials, indicating perhaps a higher temperature decomposition; however, an inflection point is observed for $3RbSH + xGeO_2 + (1-x)SiO_2 + yH_2O$ samples around ∼450 °C. The presence of this inflection point for the higher alkali content samples agrees with the conductivity data in that the thermal stability is less for these samples compared to the $2RbSH + xGeO_2 + (1-x)SiO_2 + yH_2O$ samples. This decrease in thermal stability could be due to the fact that the $3RbSH + xGeO_2 + (1-x)SiO_2 + yH_2O$ samples have more alkali modifier which acts to break up the structure, thereby reducing the thermal stability.

Conductivity Measurements. a.c. impedance measurements indicate that the substitution of Si^{4+} for Ge^{4+} reduces the proton conductivity for both the $2RbSH + xGeO_2 + (1-x)SiO_2 + yH_2O$ and $3RbSH + xGeO_2 + (1-x)SiO_2 + yH_2O$ amorphous materials. Figures 6 and 7 show the Arrhenius temperature-dependent plot of the d.c. conductivity for the as-prepared $2RbSH + xGeO_2 + (1-x)SiO_2 + yH_2O$ and $3RbSH + xGeO_2 + (1-x)SiO_2 + yH_2O$ materials, respectively. The conductivity drops over an order of magnitude at 120 °C from ∼$10^{-3.4}$ S/cm for the undoped sample, $2RbSH + GeO_2 + 1.7H_2O$, to ∼$10^{-4.5}$ S/cm for $2RbSH + 0.9GeO_2 + 0.1SiO_2 + 0.8H_2O$, respectively, using a low-pressure sealed holder for the pressed powder samples which helps to minimize effects from different thermal histories. A similar conductivity decrease was observed for
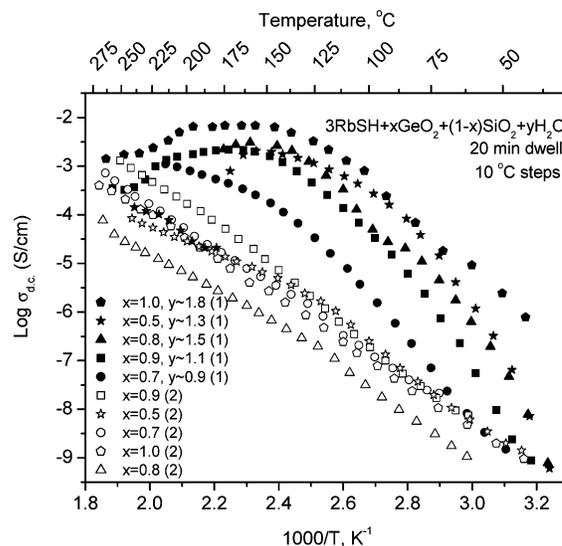
the $3RbSH + xGeO_2 + (1-x)SiO_2 + yH_2O$ samples upon substitutions of Si^{4+} for Ge^{4+}; see Figure 7. The proton conductivity at 120 °C for the undoped $3RbSH + GeO_2 + yH_2O$ sample was ∼$10^{-2.6}$ S/cm and was ∼$10^{-3.5}$ S/cm for the $3RbSH + 0.9GeO_2 + 0.1SiO_2 + 1.1H_2O$ sample. The conductivity was found to be highly dependent on both the amount of silicon and intercalated water present in the dry N_2 atmosphere. In general, as the concentration of germanium decreases, the amount of intercalated water present decreases, leading to a decrease in the proton conductivity. This result indicates that germanium plays a large role in the amount of intercalated water present in the materials which in turn plays an important role in the proton conductivities. So far, it appears that the highest proton conductivities were observed for the binary rubidium thio-hydroxogermanates, $\sigma_{d.c.} > 10^{-3}$ S/cm.

Thermal cycling of the conductivity was performed to determine the ratio of proton to alkali conductivity. The first conductivity heating cycle was performed on the as-prepared material heated from ∼25 to ∼280 °C. The cell was then cooled back to room temperature and the second run was performed on the now dehydrated material, resulting in only alkali conductivity (here rubidium) as opposed to the first cycle where it is dominated by proton motion (with some rubidium motion). It is evident from the IR spectra in Figure 2 that the presence of vibrational modes associated with $\delta(H_2O)$ modes leads to enhanced proton conductivity while samples without this peak in the IR spectra have no observable proton conductivity (i.e., their first and second cycle conductivity runs are the same). The two different possible proton conduction mechanisms are vehicle and free-proton types (Grotthuss). It is observed in these materials that as the amount of hydrated water is increased, the proton conductivity increases, indicating that the conduction method is due to this extrinsic water in a free-proton type mechanism.

a.c. impedance measurements were also performed in the presence of low levels of relative humidity (R.H.), ∼6%,

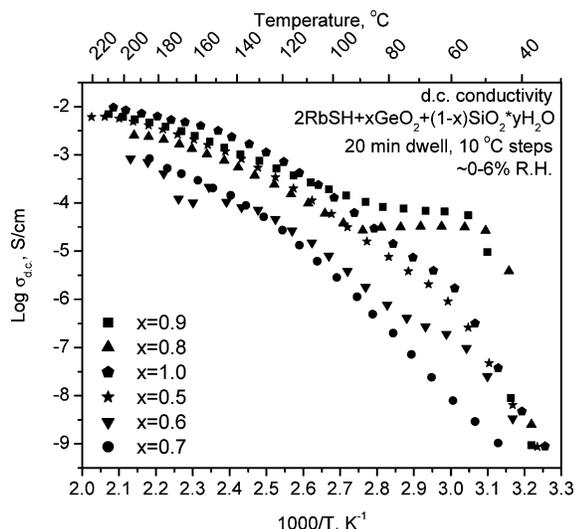**Figure 8.** Arrhenius temperature-dependent plot of d.c. conductivity values for $2RbSH + xGeO_2 + (1-x)SiO_2 + nH_2O$ at ~1 atm using ~6% R.H. produced by bubbling air through a water bath at ~50 °C.

Figure 9. Observed effects of the presence of relative humidity for $2RbSH + xGeO_2 + (1-x)SiO_2 + nH_2O$ at ~1 atm at 60 and 120 °C. The presence of humidity increases the conductivity for all samples, $0.5 \leq x \leq 1.0$.

for the $2RbSH + xGeO_2 + (1-x)SiO_2 \cdot yH_2O$ samples, Figure 8. d.c. conductivities for the low R.H. measurements of the alkali thio-hydroxosilicogermanates were dependent on the amount of SiO_2 present. For $x = 0.9$, the d.c. conductivity is between ~10^{-4} and 10^{-2} S/cm for temperatures between 60 and 200 °C, respectively (R.H. ~ 6%). Both the $x = 0.9$ and $x = 0.8$ samples show a large increase in their low-temperature conductivities with the presence of low levels of humidity. Figure 9 shows a comparison between the d.c. conductivities for both the hydrated and nonhydrated experiments at 60 and 120 °C. It is observed that the d.c. conductivity is improved at both 60 and 120 °C within the presence of hydration, once again indicating the importance of water in these systems for the proton conductivity. The large increase (~4 orders of magnitude) in the conductivity at 60 °C to ~10^{-4} S/cm makes these materials more applicable for use in proton-exchange membrane fuel cells.

Summary and Conclusions

In summary, a series of novel amorphous hydrated alkali thio-hydroxosilicogermanates of the form $zRbSH + xGeO_2 + (1-x)SiO_2 + yH_2O$ where $2 \leq z \leq 3$ and $0.5 \leq x \leq 1.0$ were synthesized from hydrothermal reactions and characterized with respect to their structure, conductivity, and thermal properties. In general, the samples were found to be X-ray amorphous with high amounts of SiO_2, resulting in semi-
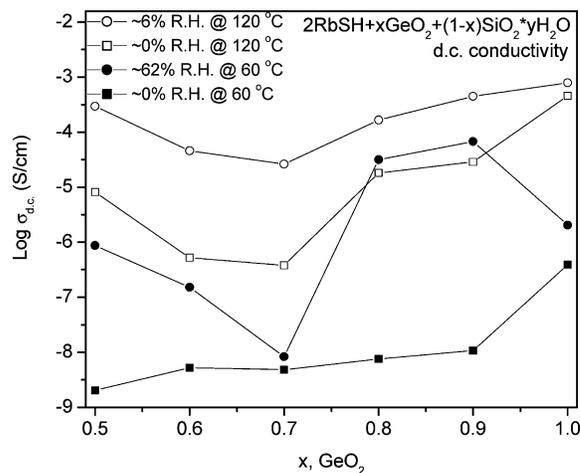
crystalline materials for $3RbSH + xGeO_2 + (1-x)SiO_2 + nH_2O$, $x = 0.6$ sample. The amorphous nature is consistent with the mechanochemical hydrothermal evaporation−precipitation synthesis method used to prepare the materials. The vibrational spectra indicate the presence of a mixed system with both germanium and silicon bonded to non-bridging oxygen and sulfur anions. There is also extensive hydrogen bonding observed through O−H stretching modes and bending modes in some samples which leads to higher proton conductivities. Maximum d.c. conductivity values of ~$10^{-4.5}$ and ~$10^{-3.5}$ S/cm at 120 °C were obtained for small SiO_2 doping amounts for $2RbSH + 0.9GeO_2 + 0.1SiO_2 + 0.8H_2O$ and $3RbSH + 0.9GeO_2 + 0.1SiO_2 + 1.1H_2O$, respectively. These conductivity values were an order of magnitude lower than that of the binary alkali thio-hydroxogermanates previously synthesized, indicating that the addition of Si^{4+} for Ge^{4+} does not weaken the electrostatic interaction between mobile cations and framework anions, but instead acts as a barrier to proton conduction. However, the presence of humidity during the d.c. conductivity experiments for $2RbSH + xGeO_2 + (1-x)SiO_2 + nH_2O$ resulted in a 4 order of magnitude increase in the proton conductivity at 60 °C to ~10^{-4} S/cm and a smaller increase at 120 °C to ~10^{-3} S/cm.